



Downscaling of CMIP5 Models Output by Using Statistical Models in a Data Scarce Mountain Environment (Mangla Dam Watershed), Northern Pakistan

Naeem Saddique^{1,2} · Christian Bernhofer¹ · Rico Kronenberg¹ · Muhammad Usman^{2,3}

Received: 30 October 2018 / Revised: 7 February 2019 / Accepted: 22 February 2019 / Published online: 8 March 2019
© Korean Meteorological Society and Springer Nature B.V. 2019

Abstract

In this study, statistical downscaling models were used to project possible future patterns of precipitation and temperature in the Jhelum River basin shared by Pakistan and India. In-situ meteorological data were used to downscale precipitation and temperature using different General Circulation Models (i.e., CanESM2, BCC-CSM1–1, and MICROC5) relative to baseline (1961–1990) under the Representative Concentration Pathway (RCP) scenarios RCP4.5 and RCP8.5. The downscaling models used were the Statistical Downscaling Model (SDSM), which uses multiple linear regression and weather generator methods, and the Long Ashton Research Station Weather Generator (LARS-WG), which uses weather generators. The results showed that the SDSM performance was slightly better than that of LARS-WG during validation and that the representation of the simulated mean monthly precipitation was more correct than that of monthly precipitation. The results also revealed that BCC-CSM1–1 performed better than CanESM2 and MICROC5 in the study region. The future annual mean temperature and precipitation are expected to rise under both RCP scenarios. The changes in the annual mean temperature and precipitation with LARS-WG were relatively higher than those with SDSM. Out of four seasons, winter and autumn are expected to be more diverse with regard to precipitation changes. However, although both models yielded non-identical results, it is certain that the basin will face a hotter climate in the future.

Keywords Downscaling models · Jhelum River basin · Weather generators · Precipitation changes

1 Introduction

Global climate has undergone a significant warming during the last five decades or so (Zhou and Yu 2006; Meehl et al. 2007). Different studies have determined that this global warming can be mainly attributed to rising greenhouse gases, particularly nitrous oxide, carbon dioxide, and ozone (Allen et al. 2000; Huang et al. 2011; Anderson et al. 2016). The

Intergovernmental Panel on Climate Change (IPCC) Fifth Scientific Assessment Report (AR5) stated that the mean global surface temperature rose by 0.85 °C (i.e., 0.65 °C to 1.06 °C) during the period of 1800–2012, and it is believed that a further increase will occur during the twenty-first century depending on four Representative Concentration Pathway (RCP) scenarios. This projected augmentation is predicted to be 0.30 °C - 1.70 °C under the RCP2.6 scenario, 1.10 °C - 2.60 °C under RCP4.5, 1.40 °C - 3.10 °C under RCP6.0 and 2.60 °C - 4.80 °C under RCP8.5 by the end of this century (IPCC 2013).

These changes in global mean temperature disturb environments, agriculture, food security, human health and ecosystems. The change in climate causes the redistribution of water resources and increases the frequency and intensity of floods and droughts (Li et al. 2013). Rainfall and temperature are more relevant parameters that directly influence the water cycle as impacts of climate change. Changes in these parameters can directly affect the amount of evapotranspiration and both the quantity and quality of the flow component. The changes

Responsible Editor: Soon-Il An.

✉ Naeem Saddique
Naeem.saddique@tu-dresden.de

¹ Institute of Hydrology and Meteorology, Technische Universität Dresden, Tharandt, Germany

² Department of Remote Sensing Am Hubland, Institute of Geography and Geology, University of Würzburg, Würzburg, Germany

³ Department of Irrigation and Drainage, University of Agriculture, Faisalabad, Pakistan

in upstream snow reserves are mostly affected by the changing climate in South Asia (Immerzeel et al. 2010). Projection of future climate change in South Asia is mandatory for exploring sustainable development and for devising future adaptation measurements to nature.

The trends of past, present and future climate change have been explored by using General Circulation Models (GCMs). These GCMs simulate the global climate on the bases of possible future greenhouse gas scenarios. The horizontal resolution of a current GCM is approximately 150 Km, and the spatial resolution of one GCM varies with respect to another (Taylor et al. 2012). Direct use of GCM for decision-making is not recommended because their output lacks fine spatial resolution, which is necessary for local applications. To surmount this gap, different downscaling techniques have been developed, including statistical approaches such as regression, stochastic weather generators and relationships with weather patterns. These downscaling techniques establish a relationship among large-scale climate variables (predictors) such as relative humidity and wind speed to local-scale variables (predictand) such as temperature and precipitation (Wilby et al. 2002; Mahmood and Babel 2013; Pervez and Henebry 2014; Zhang et al. 2016). The statistical downscaling (SD) approach does not depend on GCM boundaries, as with Regional Climate Models (RCMs). In the SD approach the biases in climatic models can be easily corrected (Wilby et al. 2002; Maraun et al. 2010; Sachindra and Perera 2016). RCMs are used in the dynamic downscaling (DD) of climatic variables and are mostly found to be heavily biased for a specific region (Turco et al. 2011), which thus necessitates the use of SD for climate change projections.

Stochastic weather generators (WGs) are probabilistic models that are used to simulate weather data at a particular place by analyzing historical climatic data and then generating a time series of weather variables with statistical properties identical to the historical data (Wilks 1999). Daily weather data generated by these models have been used in various climate change studies in agriculture and hydrology (Semenov et al. 1998; Charles et al. 2017). First order Markov chain models have been used in WGs that simulate the occurrence of rainy and dry days and use a gamma distribution for precipitation amount. Over time, second order (Mason 2004) and third order (Dubrovský et al. 2004) Markov chain models have been developed that more effectively reproduce precipitation occurrences along with climate statistics.

Regression-based downscaling methods involve establishing an empirical relationship between large scale variables (predictors) and the local past observational climate data (predictands) (Wigley et al. 1990; Dibike and Coulibaly 2005). The success of this method is depend on the quality of the data used for calibration, selection of the effective predictors and choice of the transfer function. To date, different types of regression methods, such as linear and nonlinear regression,

canonical correlation, principal component analysis and artificial neural networks, have been used to develop empirical relationships between predictand and predictors (Conway et al. 1996; Huth 2002). The main strength of regression models is that they are comparatively less difficult to apply.

The LARS-WG and SDSM are two famous statistical downscaling models used for downscaling GCM outputs such as temperature, precipitation and solar radiation. The SDSM model is a hybrid of transfer functions and WG methods. Both models have been universally used for the assessment of climate change (Wilby et al. 2002; Huang et al. 2011; Somenov and Barrow 2002; Mahmood and Babel 2013; Hassan et al. 2014; Meaurio et al. 2017; Gulacha and Mulungu 2017). The main focus of current studies is the evaluation and comparison of these models to simulate temperature and precipitation. Several findings suggest that both models perform well for simulating mean daily rainfall, although wet and dry spell lengths were better estimated by LARS-WG compared with SDSM. Similar patterns of maximum and minimum daily temperatures were found for both statistical models during calibration and validation. However, the two models did not agree for future temperature and precipitation time series due to different downscaling strategies (Dibike and Coulibaly 2005; Hassan et al. 2014).

Few recent studies have been conducted for downscaling temperature and precipitation using multiple GCMs under new RCPs scenarios for Pakistan, in particular for the Jhelum River basin (Mahmood and Jia 2017; Mahmood et al. 2018). The studies used the linear scaling method for downscaling climatic variables. Moreover, no study has been conducted using SDSM and LARS-WG under RCP scenarios until now. The aim of this study is the evaluation of both models for the study area and analysis of their output. For this purpose, two RCPs (4.5 and 8.5) and three GCMs of Coupled Model Inter-comparison Project 5 (CMIP5) were used with SDSM and LARS-WG to downscale temperature and precipitation by the end of this century. The objective of this comparison was to select the statistical method to downscale climate data that could be further used for different environmental studies. The rest of manuscript is organized as follows: section 2 states the study area and data, and section 3 gives the detailed descriptions of the two downscaling methods. Section 4 demonstrates results and discussions. The last section (section 5) illustrates the conclusions of this study.

2 Study Area and Data

2.1 Description of the Study Area

The Jhelum River basin (JRB) extends from 73 °E and 75.62 °E and 33 °N and 35 °N (Fig. 1). The basin has an area coverage of 33,397 km². Its altitude ranges from 232 to

6287 m. The upper Jhelum River is the largest tributary of the Indus Basin after the Indus River. The Jhelum River drains its water into the Mangla reservoir, the second largest reservoir in Pakistan. The majority of water flows into the reservoir during March to August, with a significant share during May due to snowmelt. More than 75% of the total water enters the reservoir during March to August (Babur et al. 2016). The total command area of the Mangla dam is 6 mha and the dam serves two purposes: it provides water for irrigation and a 6% share of the total electricity production in Pakistan (Archer and Fowler 2008). Locations of precipitation and temperature stations are shown in Fig. 1.

The Jhelum River basin is mostly covered by mountains whose altitude increases from south to north. In the southern part of the watershed, the temperature changes from subtropical and falls below the freezing point in the northern parts of the watershed during winter. The hottest months are June and July, with an average temperature of 30.5 °C, whereas the coldest months (Dec-Jan) have an average temperature of 0.3 °C. The entire JRB has a long-term mean annual rainfall of approximately 1196 mm yr⁻¹ (Table 1). Two distinct peaks can be observed based on the basin's mean precipitation,

(Fig. 2a). The highest peak in the basin is in the month of July, the result of the summer monsoon that occurs due to the energetic southwestern winds moving from the Bay of Bengal and across the Arabian Sea towards the Himalayas. The next peak (March) in the watershed is due to Western disturbances (WDs) that bring sudden winter rain (Ahmad et al. 2015).

2.2 Data

2.2.1 Meteorological Data

Observed rainfall, maximum temperature (T_{\max}) and minimum temperature (T_{\min}) data of 16 stations for the period of 1961–2012 were obtained from the Water and Power Development authority (WAPDA), Pakistan Meteorological Department (PMD), and the Indian Meteorological Department (IMD). The temperature and rainfall data of Gulmarg, Srinagar, Qaziqand, and Kupwara meteorological stations were obtained from the IMD and the remaining data from the PMD and the WAPDA.

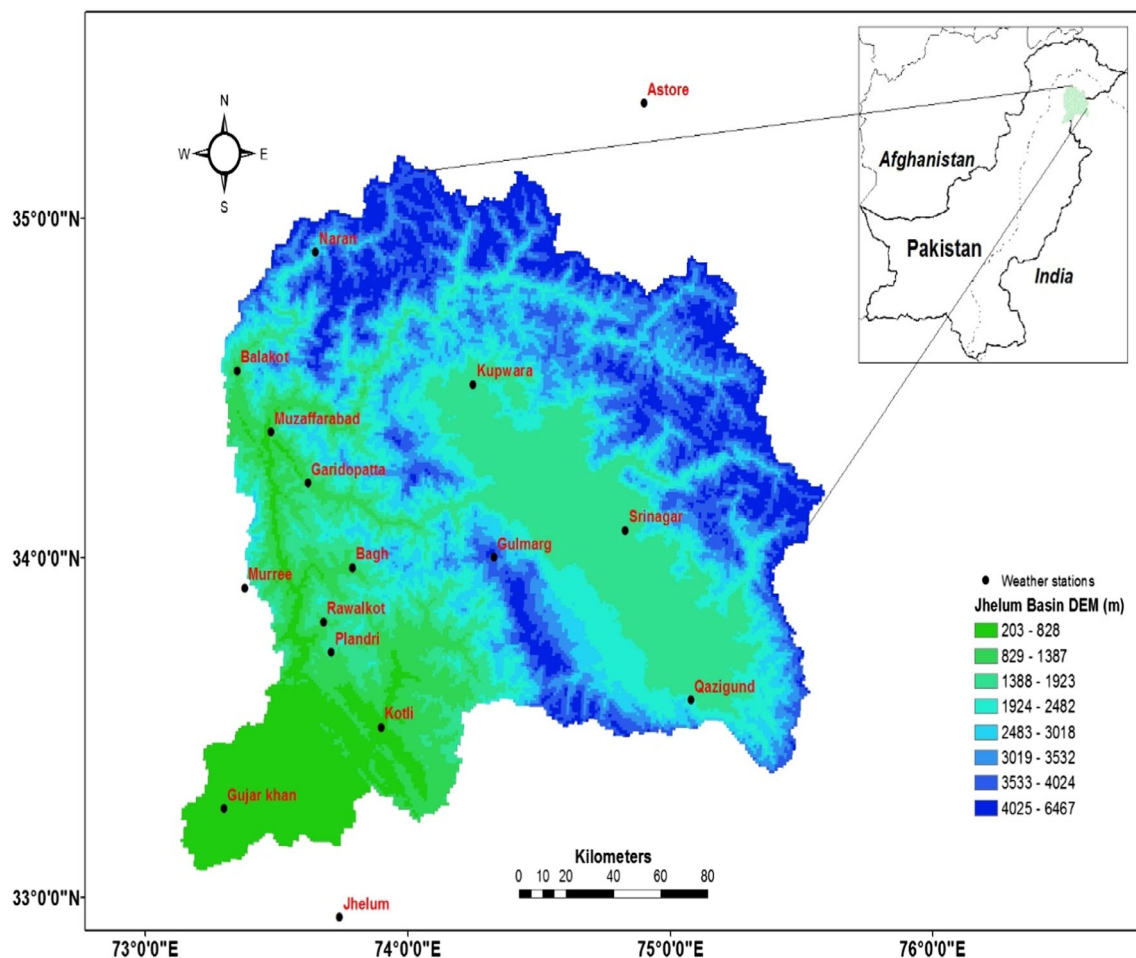


Fig. 1 Location map of the study area and weather stations

Table 1 Inventory of climate stations

Station Name	Lat (deg.)	Long (deg.)	Elve (m,MSL)	Tmax (°C)	Tmin (°C)	Precipitation (mm/year)
Jhelum	32.94	73.74	287	30.59	16.45	854
Gujar khan	33.26	73.30	458	28.02	13.98	830
Kotli	33.50	73.90	614	28.44	15.63	1245
Plandri	33.72	73.71	1401	22.73	11.30	1443
Rawalkot	33.87	73.68	1676	21.87	10.25	1397
Bagh	33.97	73.79	1067	26.80	12.86	1422
Murree	33.91	73.38	2213	16.55	8.83	1779
Garidoptta	34.22	73.62	814	25.34	12.16	1567
Muzaffarabad	34.37	73.48	702	27.32	13.55	1423
Balakot	34.55	73.35	995	25.06	11.97	1701
Naran	34.90	73.65	2362	11.13	1.15	1154
Astore	35.34	74.90	2168	15.35	3.94	534
Kupwara	34.51	74.25	1609	20.04	6.29	1245
Gulmarg	34.00	74.33	2705	11.38	1.75	1543
Srinagar	34.08	74.83	1587	19.78	7.31	721
Qaziqund	33.58	75.08	1690	19.24	6.47	1345

2.2.2 NCEP/NCAR Reanalysis Data

The daily reanalysis data for the time period of 1961–2005 were obtained from the National Centers for Environmental Prediction/National Center for Atmospheric Research (NCEP/NCAR); the data are available at a spatial coverage of 2.5 degrees longitude and 2.5 degrees latitude and include 26 atmospheric variables such as relative humidity, zonal velocity component, specific humidity, and vorticity.

2.2.3 RCP Scenario Data

Three GCM (i.e., BCC-CSM1.1, CanESM2 and MIROC5) outputs with RCP4.5 and RCP8.5 scenarios were obtained from the ESGF website (<http://pcmdi9.llnl.gov/>) for the

period of 1961–2100 and have the same number of predictors for all the GCMs and period length. RCP4.5 illustrates a medium-low RCP of radiative forcing rising to $\sim 4.5 \text{ W.m}^{-2}$ until 2070, and RCP8.5 is the highest-level RCP, which leads to radiative forcing of 8.5 W.m^{-2} by the end of twenty-first century (Moss et al. 2010). These GCMs were selected on the basis of their good performance over South Asia. All the models well captured the peaks of rainfall, specially MICRO5 performance was outstanding in highly complex climate system (Babar et al. 2015; Prasanna 2015). These GCM data were interpolated at the same grid resolution ($2.5^\circ \times 2.5^\circ$) as the NCEP data to eliminate the biases that may have occurred by contradictions present at this scale. Then, the NCEP and all the GCM predictors were normalized with the mean and standard deviation acquired from the historical

Fig. 2 Monthly mean a precipitation and rainy days and b temperature Max and Min in the Jhelum River basin

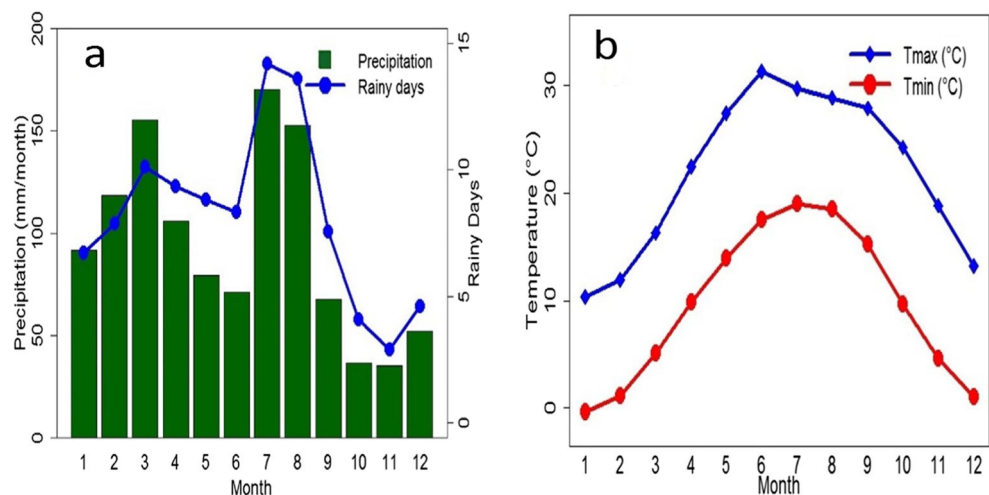


Table 2 Description of General Circulation Models (GCMs), the downscaling methods and the Representative Concentration Pathways (RCPs) used in this study

Development institute	GCM	Grid resolution	Downscaling model	RCP
Beijing Climate Center, China	BCC-CSM1–1	2.8125° × 2.8125°	SDSM	4.5
			LARS-WG	8.5
				4.5
Atmosphere and Ocean Research Institute, University of Tokyo, Japan	MIROC5	1.40625° × 1.40625°	SDSM	4.5
			LARS-WG	8.5
				4.5
Canadian Centre for Climate Modelling and Analysis, Canada	CanESM2	2.8125° × 2.8125°	SDSM	4.5
			LARS-WG	8.5
				4.5
				8.5

period of 1961–1990. Table 2 provides the overview of each GCM such as name, development institute and grid resolution.

3 Methodology

3.1 SDSM Description

SDSM is a hybrid of transfer functions and WGs (Wilby et al. 2002; Wilby et al. 2006). SDSM is extensively used worldwide to downscale weather parameters, such as temperature and precipitation, to determine how climate change affects the water cycle (Chu et al. 2010). Multiple linear regressions (MLRs) establish empirical relationships between predictors (such as geopotential height) and predictands (such as solar radiations) and generate some parameters. Weather generators use these parameters to simulate a number ensemble to create a strong correlation with station data. Three different types of sub-models can be constructed in SDSM such as monthly, seasonal and annual sub-models. The current study employs only the monthly model; 12 different regression models were developed, one for each month of the year. A conditional model was chosen for precipitation and an unconditional model for temperature (Wilby and Dawson 2004). In unconditional models a direct link is assumed between the large scale variables (predictors) and local scale variable (predictand) (e.g., local wind speeds may be a function of regional airflow indices). In conditional models, there is an intermediate process between large scale forcing and local weather (e.g., local precipitation amounts depend on the occurrence of wet-days, which in turn depend on large-scale predictors such as humidity and atmospheric pressure). A fourth order transformation was applied to precipitation data before its subsequent application in the regression analysis. For the optimization, the ordinary least squares (OLS) method was used while default

values for bias correction and variance inflation were 1 and 12, respectively. Bias correction tunes the daily downscaled temperature and precipitation, and variance inflation changes the variance in downscaled climatic data to agree more closely with observed data.

3.1.1 Screening of Predictors

The most essential component of statistical downscaling with SDSM is the screening of predictors (Wilby et al. 2002). The predictors selection method employed in the current study is consistent with those of other similar studies (Wilby et al. 2002; Khan et al. 2006; Gulacha and Mulungu 2017). In SDSM4.2, more appropriate predictors were screened based on correlation coefficient, explained variance and the p value among the individual predictors and predictand. The daily data of 26 predictors were employed to investigate correlation between predictors and predictand. The predictor with the highest correlation was selected as the first predictor (superpredictor), and the default values always had a significance level of $P < 0.05$. After the selection of the first predictor, the second and third predictors were ranked based on highest correlation and explained variance. However, in the case of precipitation, correlation between the predictand and predictors was not high (Hashmi et al. 2011; Huang et al. 2011; Meaurio et al. 2017). The predictor variables selected for precipitation and temperature in the present study are shown in bold text in Table 3.

For the selected predictors, it was observed that for both temperatures (Tmax and Tmin), temperature at 2-m height was a superpredictor, whereas two superpredictors were found for precipitation at 500 hpa, specific humidity (southwest part) and meridional wind velocity (upper part). The predictors selected in the current study are the same as in other similar studies (Wilby et al. 2002; Huang et al. 2011; Mahmood and Babel 2013).

Table 3 Overview of all NCEP variables (the one in bold text were selected for the calibration of model)

Nr.	Variable	Description
1	ncepmslpgl	Mean sea level pressure
2	ncepp1_fgl	Surface airflow strength
3	ncepp1_ugl	Surface zonal velocity
4	ncepp1_vgl	Surface meridional velocity
5	ncepp1_zgl	Surface vorticity
6	ncepp1_thgl	Surface wind direction
7	ncepp1_zhgl	Surface divergence
8	ncepp5_fgl	500 hpa air flow strength
9	ncepp5_ugl	500 hpa zonal velocity
10	ncepp5_vgl	500 hpa meridional velocity
11	ncepp5_zgl	500 hpa vorticity
12	ncepp5_thgl	500 hpa wind direction
13	ncepp5_zhgl	500 hpa divergence
14	ncepp8_fgl	850 hpa air flow strength
15	ncepp8_ugl	850hpa zonal velocity
16	ncepp8_vgl	850 hpa meridional velocity
17	ncepp8_zgl	850 hpa vorticity
18	ncepp8_thgl	850 hpa wind direction
19	ncepp8_zhgl	850 hpa divergence
20	ncepp500gl	500 hpa geopotential height
21	ncepprcpgl	Precipitation
22	nceps500gl	Specific humidity at 500 hpa
23	ncepshumgl	Surface specific humidity
24	nceprhumgl	Near surface relative humidity
25	ncepr500gl	Relative humidity at 500hpa
26	nceptempgl	Mean temperature at 2 m

3.2 Lars-WG

LARS-WG is a stochastic WG used to simulate daily time series data used in studies of the impacts of climate change (Wilks and Wilby 1999). The data simulation procedure involves three steps (Semenov and Barrow 2002). First, the LARS-WG examines the ground station parameters by obtaining their statistical properties on a monthly basis to generate probability distribution parameters for that particular site. Second, these parameters files are further used to synthesize data having the same statistical properties as the station data. LARS-WG is evaluated based on observed and simulated average monthly weather statistical indices, and relative change factors from the GCMs outputs for each month are then calculated. Finally, the calibrated parameters and relative change factors are used to project daily time series data (Wilks and Wilby 1999; Al-Safi and Sarukkalgige 2018; Sharma et al. 2018). For LARS-WG, one-year data are adequate to simulate the synthetic time series of climatic variables but the use of

more than 20 years of climate data is recommended for climate change studies (Mehan et al. 2017). The semi-empirical distribution (SED) approach is used for the length of wet and dry day series as well as daily precipitation amount. SED is normally a cumulative probability density function that has constant numerical intervals of flexible length (Semenov and Stratonovitch 2010).

In the current study, LARS-WG5.5 was used for downscaling temperature and precipitation. The model has been used with 23 intervals (ten in the old version) to illustrate the SED shape (Chen et al. 2013; Hassan et al. 2014). Therefore, the current version provides a broad range of distributions for the more-correct simulation of precipitation statistics, and the simulation of daily maximum and minimum temperature is controlled by the status of the day (i.e., whether it is wet or dry) (Al-Safi and Sarukkalgige 2018). In the present study, the model-calibrated parameters were generated for each station one by one by incorporating daily-observed data for 30 years (1961–1990). For the model validation, a 10-years long daily time series was generated using these calibrated parameters. Each of these generated daily time series was then examined to determine any statistically significant differences (at a 5% level) between the ground station and simulated weather data.

For the projection of future changes of precipitation and temperature for a weather station, the relative change factors for each month were calculated from the GCM outputs by taking differences between the data for future periods (i.e., 2011–2040, 2041–2070 and 2071–2100) and the reference period (i.e., 1961–1990). To obtain daily time series of future periods for each weather station, the calculated relative change factors were then employed for LARS-WG statistical parameters of the baseline observed data. A complete overview of the different steps used in LARS-WG applications in the development of climate change was presented in Semenov and Stratonovitch (2010).

3.3 Climate Extreme Indices

The Expert Team (ET) on Climate Change Detection and Indices (ETCCDI) jointly sponsored by the World Meteorological Organization (WMO) Commission of Climatology (CCI) and the Climate Variability and Predictability (CLIVAR) project developed 27 indices for monitoring the changes in climate extremes (Peterson 2005). The computation of these indices requires daily precipitation and temperature (minimum and maximum) dataset. In this study, we considered only 4 indices for models evaluation (listed in Table 4).

3.4 Model Performance

The performances of the SDSM and LARS-WG statistical models were examined by comparing the downscaled and

Table 4 Core climate indices calculated and analyzed in this study

Sr. No.	Index	Index long name	Index detail	Units
1	SU	Number of summer days	Annual account of days when TX (daily maximum temperature) >25 °C	Days
2	CWD	Consecutive wet days	Maximum number of consecutive days with RR ≥ 1 mm	Days
3	CDD	Consecutive dry days	Maximum number of consecutive days with RR < 1 mm	Days
4	R10	Number of heavy precipitation days	Annual account of days when RR ≥ 10 mm	Days

observed precipitation, T_{\max} and T_{\min} , by using different statistics: the correlation coefficient (R), Bias, Percent of bias (Pbias), Root Mean Square Error (RMSE) and Normalized Root Mean Square Error (NRMSE).

$$R = \frac{\sum_{i=1}^N (P_i - \bar{P}) \cdot (O_i - \bar{O})}{\sqrt{\sum_{i=1}^N (P_i - \bar{P})^2} \cdot \sqrt{\sum_{i=1}^N (O_i - \bar{O})^2}} \quad (1)$$

$$Bias = \frac{\sum_{i=1}^N (P_i - O_i)}{N} \quad (2)$$

$$Pbias = \frac{\sum_{i=1}^N (P_i - O_i)}{\sum_{i=1}^N O_i} \times 100 \quad (3)$$

$$RMSE = \frac{\sqrt{\sum_{i=1}^N (O_i - P_i)^2}}{\sqrt{N}} \quad (4)$$

$$NRMSE = \frac{RMSE}{\bar{O}} \times 100 \quad (5)$$

where O_i and P_i are the observed and modeled values, respectively, \bar{O} and \bar{P} are the means of the observed and modeled values, respectively, and N is the number of data points. A Taylor diagram (Taylor 2001) is used to quantify the statistical relationship between observed and modeled data. In this diagram, the relationship is explained by the Pearson correlation coefficient (R), the standard deviation () and the centered root mean square difference (RMS).

Table 5 Performance of the models during the calibration period

		\bar{X}	R^2	RMSE	Bias	Pbias (%)	SD
Precipitation (mm/month)	OBSERVED	92.66					44.97
	SDSM	95.01	0.994	3.86	2.31	2.50	44.70
	LARS-WG	99.57	0.942	12.90	6.88	7.42	39.98
T_{\max} (°C/month)	OBSERVED	21.856					7.515
	SDSM	21.829	0.998	0.252	-0.027	-0.127	7.467
	LARS-WG	21.861	0.995	0.721	0.004	0.021	7.271
T_{\min} (°C/month)	OBSERVED	9.617					7.183
	SDSM	9.659	0.998	0.260	0.041	0.442	7.157
	LARS-WG	9.693	0.990	0.704	0.075	0.787	6.980

4 Results and Discussion

4.1 Calibration of SDSM and LARS-WG

In this study the calibration period for both models was 30 years (1961–1990). The downscaled mean monthly precipitation, temperature maximum and minimum simulated by both models are shown in Table 5. In the case of T_{\max} and T_{\min} , both models behaved very close to the observed data, whereas the RMSE value of SDSM was lower than that of LARS-WG, which shows the better performance of SDSM. However, the Pbias values for SDSM and LARS-WG were -0.127% and 0.021%, respectively. With respect to precipitation, SDSM produced much better results than LARS-WG. The simulated average monthly precipitation values of SDSM and LARS-WG were approximately 2.35 mm and 6.91 mm higher compared with the mean (\bar{X}) observed value. The values of RMSE and R^2 represents the satisfactory performance of LARS-WG in downscaling the precipitation.

Although the SDSM performed better in the statistical comparison, the predicted SDSM data were not fully able to capture the observed mean monthly weather data (i.e., Fig. 3). It is seen that both models overestimated the rainfall in almost all months. However, LARS-WG overestimated more as compared with SDSM in all months except February and December. Two peaks can be observed in the trend, one in March and the other in July. The March peak was well captured by LARS-WG and the other peak by SDSM. In term of T_{\max} and T_{\min} , the LARS-WG and SDSM overestimated

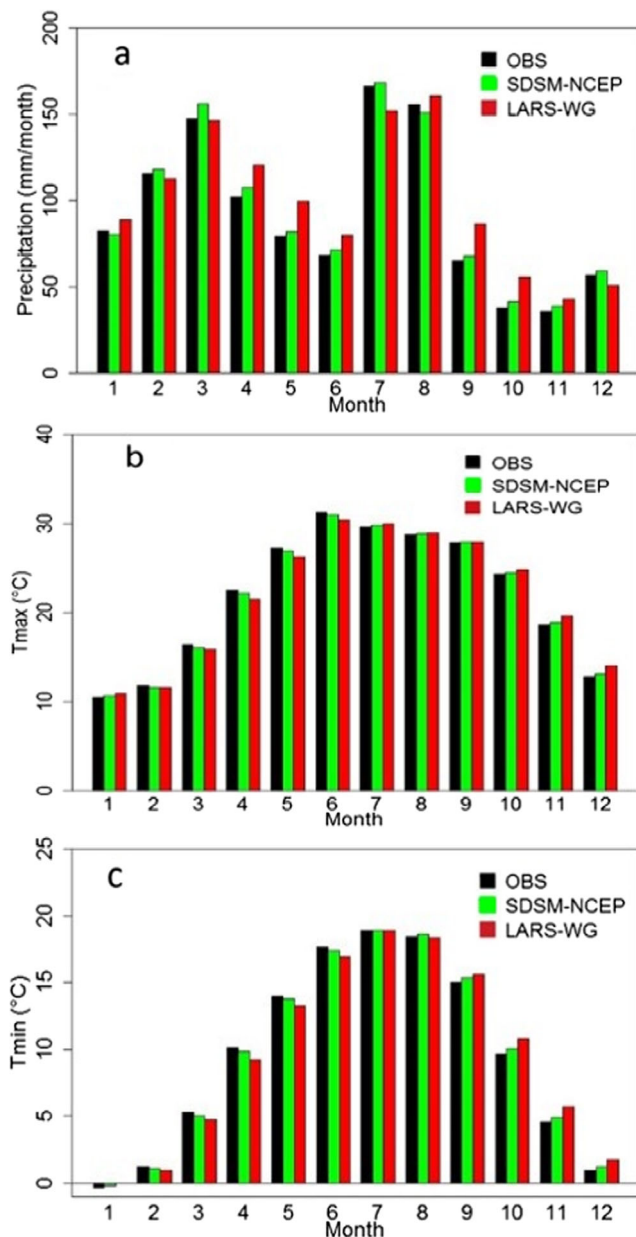


Fig. 3 SDSM and LARS-WG calibration results for **a** Precipitation, **b** Tmax and **c** Tmin in the Jhelum River basin

temperatures in the months of January, October, November and December and underestimated them in the months of February, March, April, May and June.

4.2 Validation of Downscaling Models

Five datasets were generated for the historical period 1991–2000 to validate the SDSM and LARS-WG models. For SDSM forcing of NCEP, three GCM, BCC-CSM 1–1, MIROC5 and CanESM2 variables were used, denoted as SDSM-NCEP, SDSM-BCC, SDSM-MIROC and SDSM-

Can, respectively. To validate the LARS-WG model the same statistical indicators of observed data in calibration were used without any forcing applied.

4.2.1 Comparisons of Model Performance

In the validation period, the performances of both statistical models were statistically assessed by using NRMSE and Pbias between the observed and downscaled data for precipitation, Tmax and Tmin. The results presented in Table 6 are the calculated mean values of all meteorological stations. It can be seen that daily precipitation simulated by SDSM and LARS-WG show mean NRMSE values of 100.8 and 107.8%, respectively. In monthly precipitation by SDSM, NRMSE and Pbias range from 66.3 to 73.0% and -2.1 to -9.1% , respectively. Conversely, LARS-WG has NRMSE and Pbias values of 73.8% and -5.7% , respectively. Higher value of NRMSE show that LARS-WG underperformed for downscaling both daily and monthly precipitation. With regard to mean monthly precipitation, LARS-WG has an NRMSE value again higher than SDSM, which indicates that SDSM performed better in downscaling the precipitation in the study area than LARS-WG. In the downscaling of monthly (10 years = $10 \times 12 = 120$ months) and mean monthly (10 years = mean 12 months) precipitation, the NRMSE and Pbias of SDSM-BCC were less than those of SDSM-MIROC and SDSM-Can.

In the case of daily temperature (both Tmax and Tmin) simulated by SDSM and LARS-WG, NRMSE ranged from 20.1 to 27.6% and 24.5 to 31.1%, respectively. In the simulation of monthly temperature (both Tmax and Tmin), SDSM, NRMSE and Pbias ranged from 8.5 to 18.8% and -0.1 to 1.3%, respectively, and in LARS-WG these values ranged from 12.3 to 16.2% and 0.1 to 3.1%, respectively. In addition, for mean monthly Tmax and Tmin for SDSM-NCEP (including SDSM-BCC, MIROC and Can), NRMSE ranged from 2.7 to 10.6% and LARS-WG presented a good simulation, with NRMSE ranging from 7.5 to 7.9%. In the downscaling of precipitation and temperature, BCC-CSM1–1 GCM performance was better than that of the other GCMs. SDSM performance was better with NCEP reanalysis data than from Can, MIROC and BCC because NCEP data were used during model calibration.

4.2.2 Taylor Diagram

The Taylor diagram provides a brief statistical summary of standard deviation, correlation coefficient and root mean square difference. Figure 4 shows the performance of SDSM and LARS-WG for the downscaling of daily, monthly and mean monthly temperature and precipitation. For daily precipitation, SDSM with NCEP has a correlation coefficient greater than 0.2, whereas LARS-WG has a correlation coefficient less

Table 6 Models performance during the validation period

	Precipitation		Tmax		Tmin	
	NRMSE (%)	Pbias (%)	NRMSE (%)	Pbias (%)	NRMSE (%)	Pbias (%)
Daily						
SDSM-NCEP	100.8	-5.1	27.6	0.6	20.1	6.4
LARS-WG	107.8	-3.4	31.2	1	24.5	8.4
Monthly						
SDSM-NCEP	67.1	-7.3	12.9	0.2	8.5	1.3
LARS-WG	73.8	-5.7	16.2	0.5	12.3	3.1
SDSM-Can	71.6	-8.1	17.6	-0.3	12.8	-1.2
SDSM-MICROC	73.0	-9.1	18.8	-0.7	13.1	-0.4
SDSM-BCC	66.3	-2.1	16.7	-0.1	12.1	0.1
Mean Monthly						
SDSM-NCEP	14.5	-0.1	3.6	0.2	2.7	0.6
LARS-WG	30.8	1.0	7.9	0.6	7.5	2.5
SDSM-CanESM2	28.6	-1.9	10.1	-0.3	9.1	-1.8
SDSM-MICROC5	28.4	-2.9	10.6	-0.6	7	-1
SDSM-BCC	26.9	-0.5	5.8	0.1	5.9	-0.7

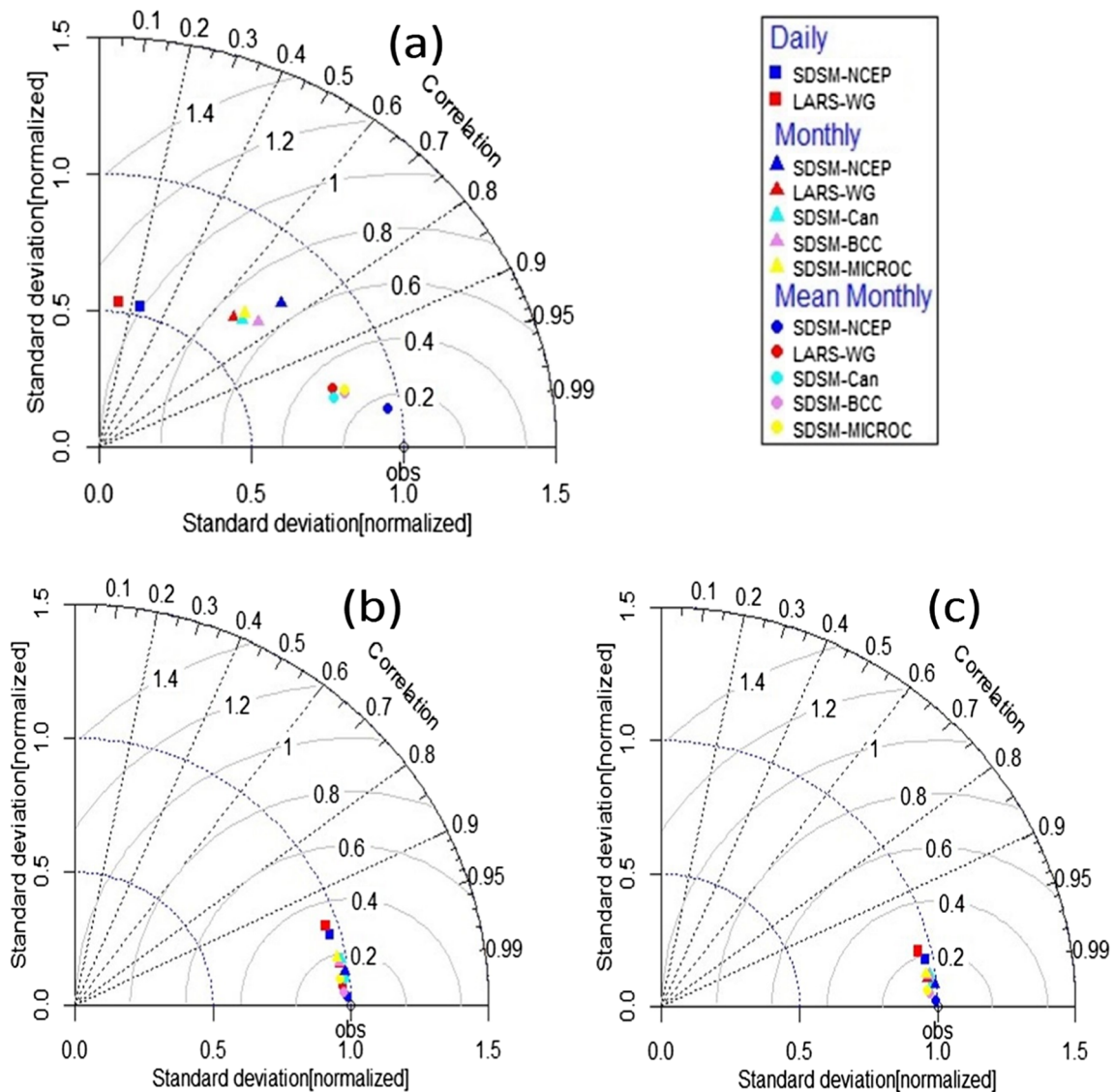
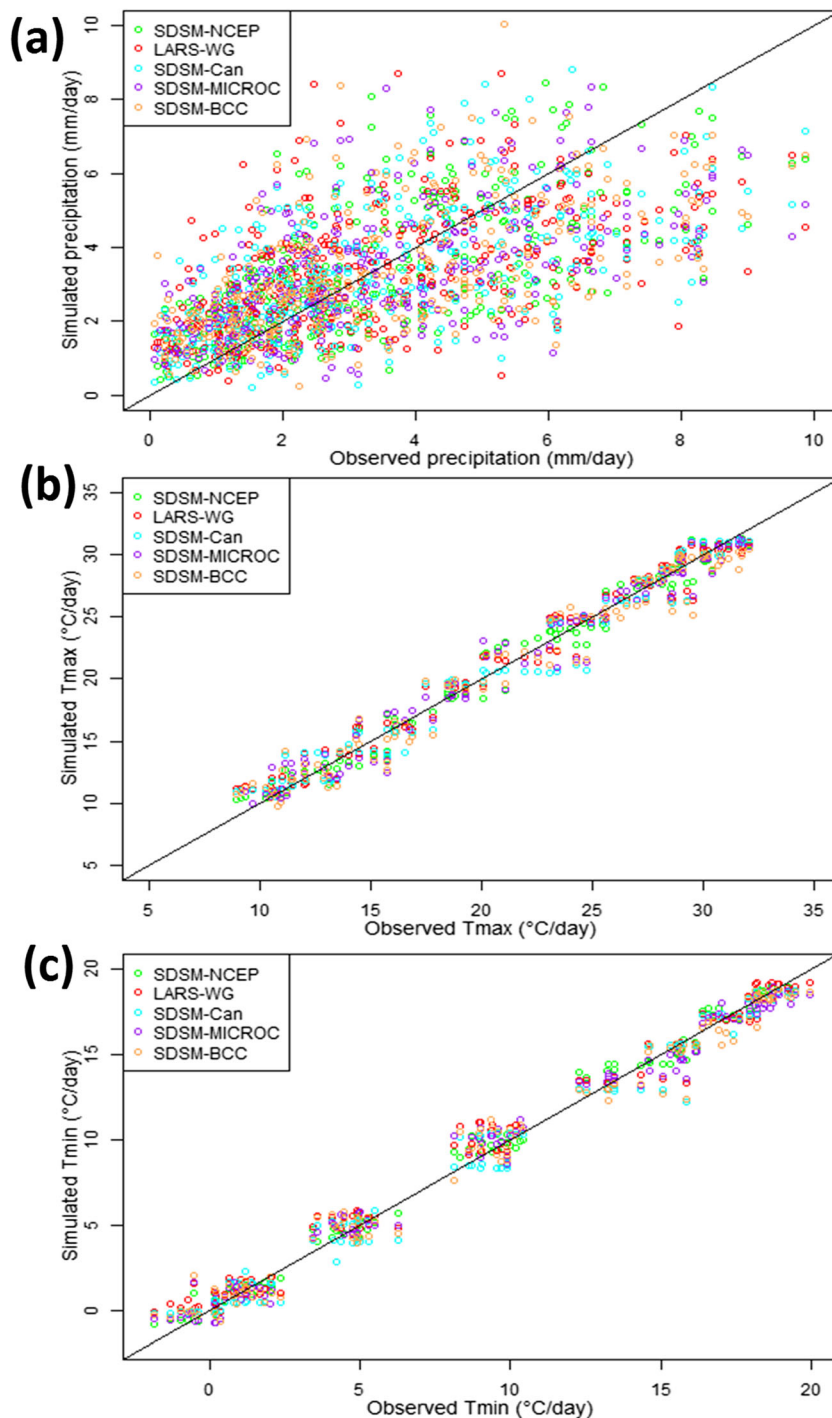


Fig. 4 Taylor diagram for three GCMs during SDSM and LARS-WG validation for **a** Precipitation, **b** Tmax and **c** Tmin in the Jhelum River basin

than 0.15. As usual, the downscaling of daily time series precipitation is not easy, and the simulation results for daily precipitation in this study are comparable with those of a few past studies (Huang et al. 2011; Hassan et al. 2014). Simulation results for monthly precipitation by SDSM show correlation coefficient values in the range of 0.65 to 0.80, whereas these values are less than 0.65 for LARS-WG. For mean monthly precipitation, the SDSM-NCEP model result standard deviation was very close to the observed data. The normalized RMS

difference between simulated and observed data was less than 0.2 (i.e., 6.96 mm), and the correlation coefficients of all SDSM models (BCC, Can, and MICROC) were in the range of 0.95 to 0.99, which shows that the performance of SDSM is relatively better than that of LARS-WG. For daily Tmax and Tmin, SDSM and LARS-WG correlation coefficients were greater than 0.95 and the normalized RMS differences were less than 0.4. Mean monthly temperature is thus better projected than monthly data.

Fig. 5 Scatter plot observed versus simulated values during SDSM and LARS-WG validation for **a** Precipitation, **b** Tmax and **c** Tmin in the Jhelum River basin



4.2.3 Scatter Plot

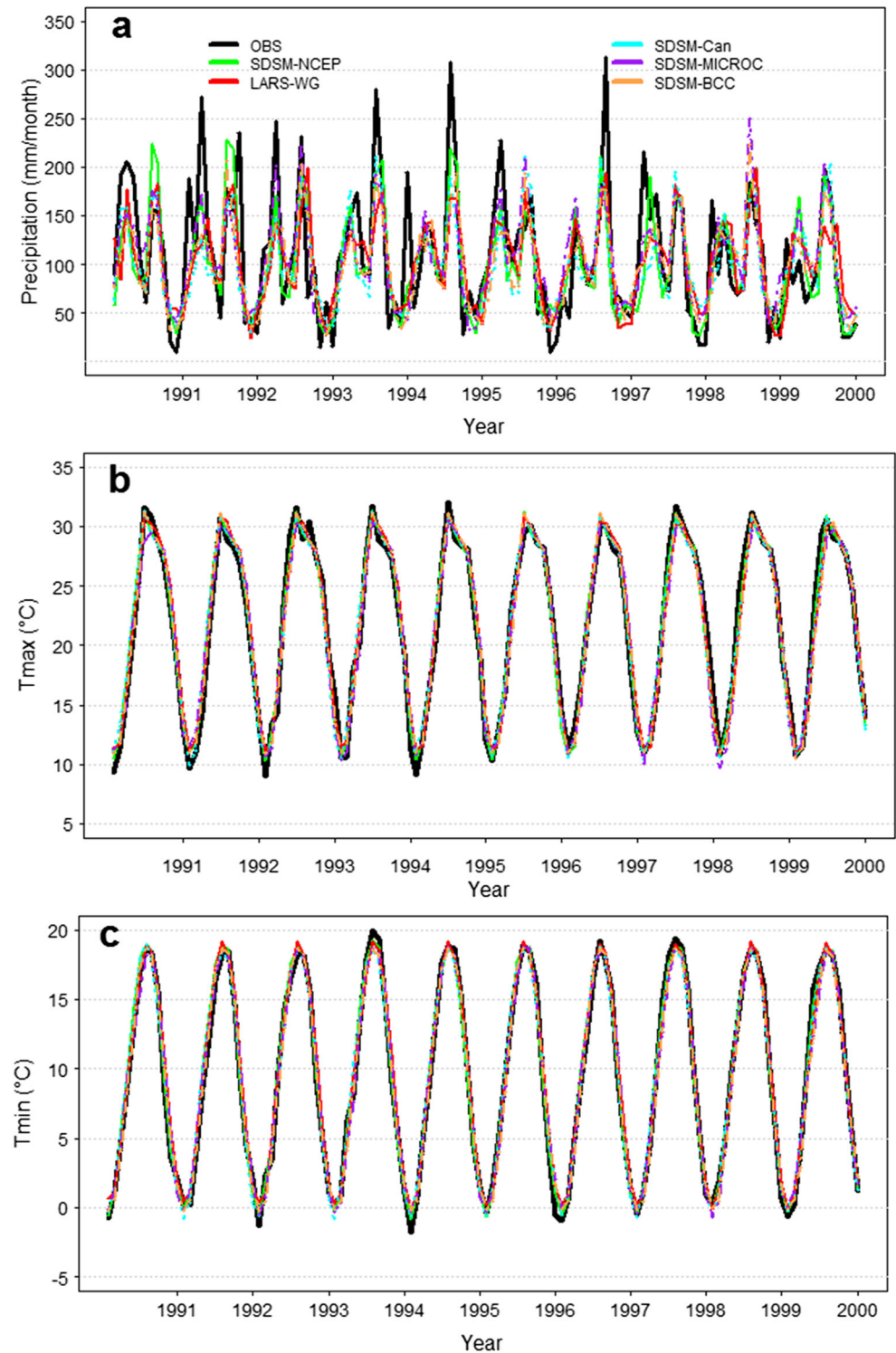
Scatter plot between mean daily observed and simulated values are shown in Fig. 5. It is seen that all the data sets (LARS-WG, SDSM-NCEP, SDSM-BCC, SDSM-MIROC and SDSM-Can) are not able to simulate the daily precipitation time series very well. In the case of temperature (both

Tmax and Tmin), it can be observed that there is a satisfactory agreement between the observed and simulated daily values.

4.2.4 Temporal Variation in Precipitation and Temperature

Figure 6 shows the comparison of monthly downscaled and observed precipitation. It is obvious that both the

Fig. 6 Monthly results of SDSM and LARS-WG during validation for **a** precipitation, **b** Tmax and **c** Tmin in the Jhelum River basin



models fairly captured the precipitation peaks (though in some years under estimation) and they well reproduce temporal variation in precipitation. However, the other three data sets of SDSM (i.e., BCC, MICROC and Can) also display good overlapping with observed precipitation with small under estimation. The trend of LARS-WG in all months of the year was similar to the three data sets of SDSM, with comparatively more deviation from observed precipitation. The datasets of SDSM and LARS-WG are displayed to emulate Tmax and Tmin, climatologies with good precision, yet there are very small over estimated and under estimated biases.

4.2.5 Observed and Simulated Climate Indices

Figure 7 shows the comparison of mean values of climate indices of simulated temperature and precipitation with observed data for the validation period. The summer days (SU) and heavy precipitation days (R10) were well simulated by SDSM and LARS-WG. It can be seen that

consecutive wet days (CWD) are overestimated by SDSM-NCEP while SDSM with other datasets well simulate the CWD. Consecutive dry days (CDD) were slightly overestimated by both the models.

4.3 Future Climate Change

In this study, the future period was divided into three periods: 2011–2040 (2020s), 2041–2070 (2050s), and 2071–2100 (2080s).

4.3.1 Changes in Seasonal and Annual Precipitation

Table 7 shows the projected change in mean annual precipitation. All GCMs projected an increase in precipitation under both downscaling methods, two RCPs and three future periods relative to the baseline. For SDSM the mean annual precipitation changes for the three GCMs ranged from 4.4 to 8.3%, 7.3 to 10.6% and 6.4 to 12.9% under RCP4.5 during the 2020s, 2050s, and 2080s, respectively, whereas under RCP8.5 these changes ranged from 4.5 to 8.7%, 7.9 to

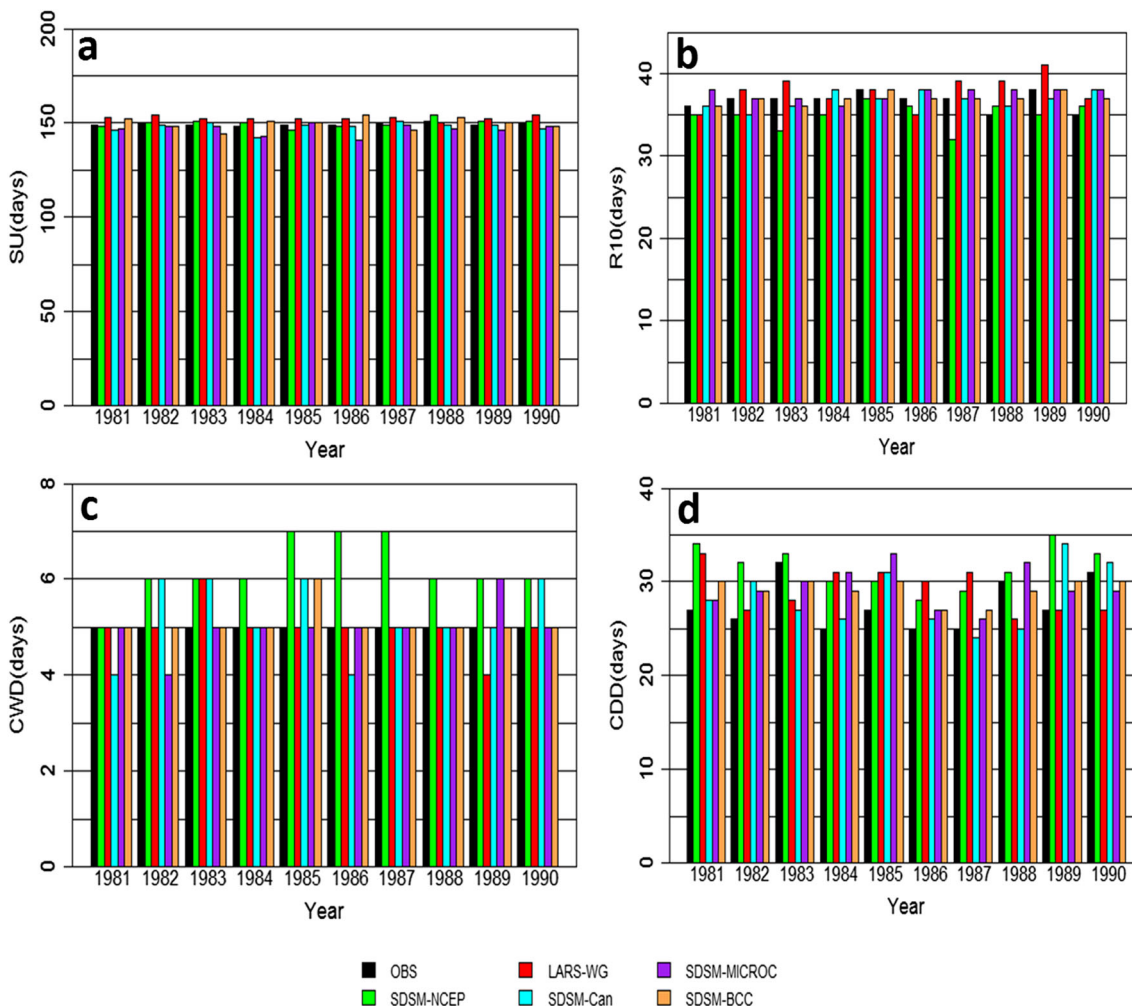


Fig. 7 Mean values of extreme indices for the validation (1991–2000) climate

Table 7 Annual changes in Precipitation (%) in three future periods under three GCMs and two scenarios (RCP4.5 and RCP8.5) with two models

Periods	SDSM			LARS-WG		
	CanESM2	BCC-CSM1-1	MICROC5	CanESM2	BCC-CSM1-1	MICROC5
RCP4.5						
2020s	8.3	6.9	4.4	14.6	16.4	11.6
2050s	10.6	8.6	7.3	17.9	21.6	16.4
2080s	12.9	6.4	8.3	22.5	25.3	20.7
RCP8.5						
2020s	8.7	4.5	6.9	16.6	13.1	16.6
2050s	12.3	7.9	10.2	22.1	22.9	23.5
2080s	16.9	11.6	17.9	32.2	24.5	28.2

12.3%, and 11.6 to 17.9% during the three future periods, respectively. The mean annual precipitation predicted by using LARS-WG showed a significant increase in precipitation in all GCMs. The three GCMs generated increments ranging from 11.6 to 16.4%, 16.4 to 21.6%, and 20.7 to 25.3% under RCP4.5, whereas under RCP8.5 these changes ranged from 13.1 to 16.6%, 22.1 to 23.5%, and 24.5 to 32.2%, respectively, during the three future periods. Mean annual precipitation projected by the BCC-CSM1-1 GCM in RCP8.5 was slightly less in magnitude compared with RCP4.5 in both downscaling methods for two future periods. Among the future years, CanESM2, BCC-CSM1-1 and MICROC5 with two downscaling methods and two RCPs showed the highest change in values in the 2080s.

The changes in seasonal mean precipitation under two scenarios using SDSM and LARS-WG for the 2080s are shown in Fig. 8. It is seen that under RCP4.5, the seasons in which changes of mean precipitation would be extreme in the 2080s were winter and autumn. During autumn, a dramatic increase in precipitation was found using both downscaling methods. This increment would shift the monsoon period in the study area; similar findings are found under RCP8.5 but with differences in magnitude for the change. The magnitude of the

predicted change for the seasonal and annual mean precipitation for the three GCMs and two scenarios using LARS-WG were greater compared with SDSM.

4.3.2 Changes in Seasonal and Annual Tmax

Table 8 illustrates the changes in Tmax during three future periods using RCP4.5 and RCP8.5 for both models relative to a baseline (1961–1990). By using the SDSM and LARS-WG methods, the projected Tmax showed an increase ranging between 0.40 and 1.38 °C, 0.81 and 2.27 °C, and 1.07 and 4.18 °C for the future periods, respectively (i.e., the 2020s, 2050s, and 2080s). A continuously increasing trend was projected for Tmax by all GCMs, two RCPs and both downscaling methods in the future periods. The RCP8.5 scenarios using SDSM and LARS-WG projected higher increases in Tmax than the future RCP4.5 scenarios except during the 2020s by MICROC5 in SDSM. The highest positive change in temperature was found in the 2080s and the change in magnitude for Tmax was higher for LARS-WG compared with SDSM for all GCMs.

The seasonal changes of Tmax in the 2080s under two scenarios using SDSM and LARS-WG are shown in Fig. 9.

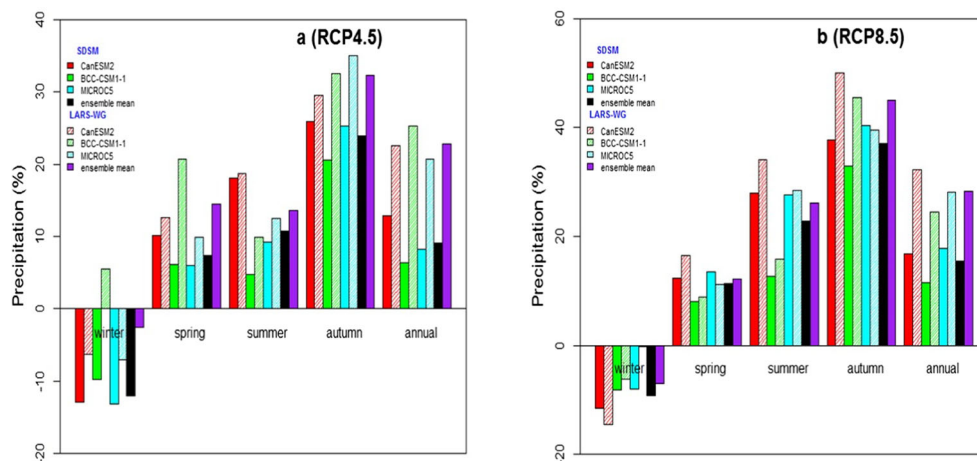
Fig. 8 Change in seasonal and annual mean precipitation in percentage (relative to baseline) with SDSM and LARS-WG in the 2080s under **a** RCP4.5 and **b** RCP8.5

Table 8 Annual changes in Tmax (°C) using three GCMs and two scenarios (RCP4.5 and RCP 8.5) with two models

Periods	SDSM			LARS-WG		
	CanESM2	BCC	MICROC5	CanESM2	BCC	MICROC5
	RCP4.5					
2020s	0.40	0.49	0.64	0.69	0.67	0.70
2050s	0.83	0.81	1.08	1.02	1.29	1.38
2080s	1.07	1.09	1.32	1.98	2.18	1.77
RCP8.5						
2020s	0.72	0.52	0.52	0.97	0.92	1.38
2050s	1.32	0.88	1.29	1.56	2.21	2.27
2080s	2.09	1.16	2.02	3.31	4.18	3.54

It can be seen that under RCP4.5 three seasons showed increments in Tmax with different magnitudes but a decreasing trend was found in spring with SDSM in all GCMs. Under the RCP8.5 scenario for both downscaling models, the three GCMs projected increased temperature in all seasons except for summer by BCC-CSM1-1 GCM. Autumn showed maximum increases in Tmax under both RCPs.

4.3.3 Changes in Seasonal and Annual Tmin

Table 9 represents the changes in Tmin in three future time periods relative to the baseline period using the SDSM and LARS-WG models. The increase in projected Tmin ranged between 0.3 and 1.5 °C, 0.9 and 2.3 °C and 1.1 and 4.2 °C for the future periods, respectively (i.e., the 2020s, 2050s, and 2080s). For annual mean Tmin, the BCC-CSM1-1 showed the largest increase during the 2080s under the two downscaling methods and all scenarios.

The seasonal changes of Tmin in the period of the 2080s using RCP4.5 and RCP8.5 with the SDSM and LARS-WG models are shown in Fig. 10. Under RCP4.5, SDSM with all the GCMs predicted decreases in Tmin in spring, and BCC-CSM1-1 predicted more increases of temperature in all

Table 9 Annual changes in Tmin (°C) using three GCMs and two scenarios (RCP4.5 and RCP 8.5) with two models

Periods	SDSM			LARS-WG		
	CanESM2	BCC	MICROC5	CanESM2	BCC	MICROC5
	RCP4.5					
2020s	0.5	0.7	0.3	0.7	0.9	0.8
2050s	0.9	1.2	0.9	0.9	1.5	1.5
2080s	1.1	1.4	1.1	1.9	2.2	1.9
RCP8.5						
2020s	0.6	0.8	0.5	0.9	1.5	1.4
2050s	1.2	1.6	1.2	1.5	2.3	2.3
2080s	1.9	1.9	1.9	3.0	4.2	3.6

seasons. Under RCP8.5, all seasons showed increments in Tmin in the 2080s, although with different magnitudes. SDSM and LARS-WG predicted that the most-warmed season in the 2080s would be autumn, with a rise of mean Tmin between 4.11 and 4.66 °C.

5 Conclusions

The performances of a multi-regression model called SDSM, a weather generator called LARS-WG and three GCMs (CanESM2, BCC-CSM1-1 and MICROC5) were evaluated with respect to their ability to downscale precipitation, Tmax and Tmin for two RCPs (RCP4.5 and RCP8.5) for the Jhelum River basin. The screening of the most suitable predictors of SDSM was very challenging in the study area due to complex topography. There is little accordance of opinions on the best method of selecting predictors for climatic variables, especially for rainfall. The meridional velocity (at 500 hpa) was found to be a superpredictor for rainfall for most weather stations in the Jhelum River basin.

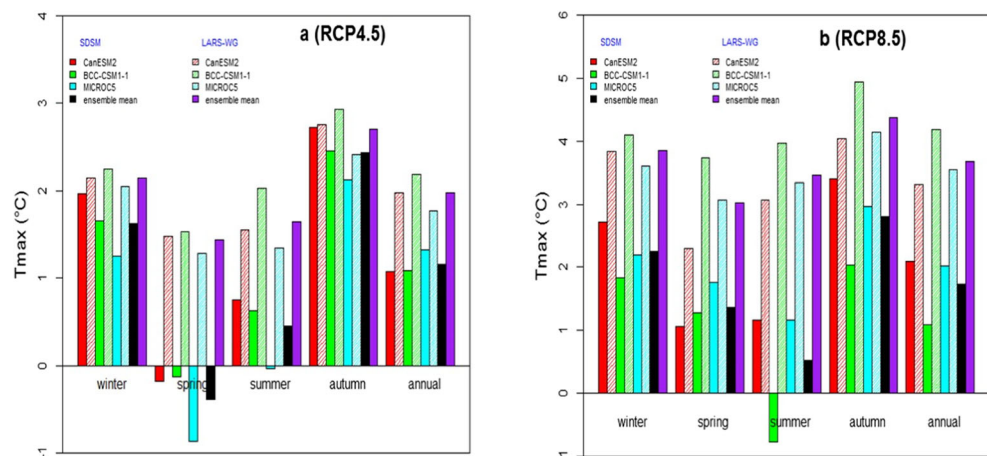
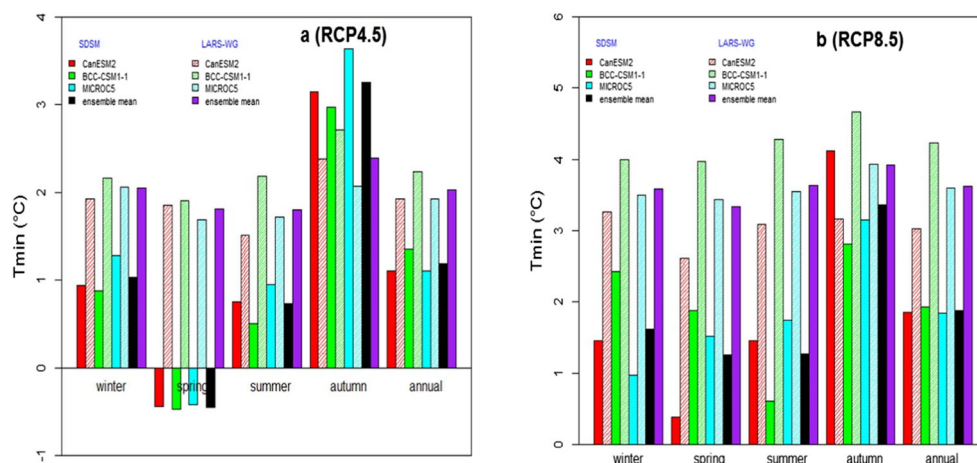
Fig. 9 Change in seasonal and annual mean Tmax (relative to baseline) with SDSM and LARS-WG in the 2080s under **a** RCP4.5 and **b** RCP8.5

Fig. 10 Change in seasonal and annual mean Tmin (relative to baseline) with SDSM and LARS-WG in the 2080s under **a** RCP4.5 and **b** RCP8.5



The results showed that during calibration, the simulation of mean monthly precipitation SDSM performance was better than that of LARS-WG, although, graphically, both models slightly overestimated the rainfall with different magnitudes. However, for Tmax and Tmin the simulated results for both models were very close to observations. During validation, the precipitation downscaled by SDSM with NCEP data was good compared with the results of LARS-WG, especially in modelling the mean monthly precipitation, for which the correlation value was higher than 0.98. A good performance of the BCC-CMS1–1 global climate model was found in downscaling of the monthly and mean monthly precipitation. Overall, the validation results show that SDSM and LARS-WG could be used for future projection using all three GCM outputs.

The data were divided into three periods (the 2020s, 2050s and 2080s) to observe the changes in future simulated data. The results of the three future periods showed that annual mean basin precipitation increased with both statistical downscaling approaches, three GCMs and with RCP4.5 and RCP8.5. The predicted change in precipitation with LARS-WG was higher in magnitude than that of SDSM. In the 2080s, the annual mean precipitation of the Jhelum River basin under RCP4.5 and RCP8.5 would increase by 12.7% and 17.9%, respectively, with SDSM, which were higher than the simulation results presented in another study (Mahmood and Babel 2013) for the same region. Significant seasonal variations in precipitation change would be observed when compared with the baseline period; all the seasons except winter showed increments in precipitation in the 2080s under both RCPs, three GCMs with SDSM and LARS-WG. Autumn showed a higher percentage increase in precipitation compared with spring and summer. The BCC-CSM1–1 GCM projected less percentage increase under both RCPs with SDSM compared with the other two GCMs, and the reverse was the case for LARS-WG. The AR5 (models

average) also reported an increase in precipitation in the study area for the future time period (IPCC 2013).

For temperature (Tmax and Tmin), both downscaling approaches showed annual increases in temperature in the study area with RCP4.5 and RCP8.5. However, the results showed that the magnitudes of temperature changes using both approaches were significantly different from each other. The results on a seasonal basis also showed increments in temperature in all seasons under RCP8.5; however, the temperature in spring would be decreased with both approaches and the three GCMs under RCP4.5. The results showed a maximum increment in temperature in the study area of 4.7 °C (autumn).

In general, the SDSM and LARS-WG models well simulated the present day temperature, although the precipitation results of SDSM were reasonably better than those from LARS-WG. Future results for both the models were significantly different from each other due to their different downscaling strategies and concepts. The BCC-CSM1–1 GCM model performed better than the other GCMs. From the downscale results, it is concluded that the Jhelum basin will face more rainfall in the future. All the GCMs also showed increments in Tmax and Tmin, which will most likely result in a hotter climate of the region in the future with respect to the current climate. These results contribute to later scientific work such as water resources planning and in the agriculture sector. However much more research is needed with maximum number of GCMs to understand the uncertainties related to these climate models.

Acknowledgements We are thankful to the Institute of Hydrology and Meteorology, Chair of Meteorology, Technical University Dresden for giving the opportunity to perform this research. Mr. Naeem Saddique also acknowledge the Higher Education Commission of Pakistan (HEC) Pakistan and German Academic Exchange Service (DAAD) Germany for providing him financial support for his PhD studies. The financial support for this project was extremely useful for the completion of this research endeavor and is greatly appreciated. The authors wish to extend a special thanks to the organizations WAPDA, PMD and IMD for providing access to meteorological data utilized in this research.

Publisher's Note Springer Nature remains neutral with regard to jurisdictional claims in published maps and institutional affiliations.

References

- Ahmad, I., Ambreen, R., Sun, Z., Deng, W.: Winter-spring precipitation variability in Pakistan. *Earth Environ. Sci.* **4**(1), 115–139 (2015). <https://doi.org/10.4236/ajcc.2015.41010>
- Allen, M., Stott, P., Mitchell, J., Schnur, R., Delworth, T.: Quantifying the uncertainty in forecasts of anthropogenic climate change. *Nature*. **407**(6804), 617–620 (2000). <https://doi.org/10.1038/35036559>
- Al-Safi, H.I.J., Sarukkalige, P.R.: The application of conceptual modelling to assess the impacts of future climate change on the hydrological response of the Harvey River catchment. *J. Hydro Environ. Res.* (2018). <https://doi.org/10.1016/j.jher.2018.01.006>
- Anderson, T.R., Hawkins, E., Jones, P.D.: CO₂, the greenhouse effect and global warming: from the pioneering work of Arrhenius and Callendar to today's earth system models. *Endeavour*. **40**(3), 178–187 (2016). <https://doi.org/10.1016/j.endeavour.2016.07.002>
- Archer, D.R., Fowler, H.J.: Using meteorological data to forecast seasonal runoff on the river Jhelum, Pakistan. *J. Hydrol.* **361**(1–2), 10–23 (2008). <https://doi.org/10.1016/j.jhydrol.2008.07.017>
- Babar, Z.A., Zhi, X.F., Fei, G.: Precipitation assessment of Indian summer monsoon based on CMIP5 climate simulations. *Arab. J. Geosci.* **8**(7), 4379–4392 (2015). <https://doi.org/10.1007/s12517-014-1518-4>
- Babur, M., Babel, S., Shrestha, S., Kawasaki, A., Tripathi, N.K.: Assessment of climate Change impact on reservoir inflows using multi climate-models under RCPs—the case of Mangla dam in Pakistan. *Water*. **8**(9), 389 (2016). <https://doi.org/10.3390/w8090389>
- Charles, B.C., Elijah, P., Vernon, R.N.C.: Climate change impact on maize (*Zea mays* L.) yield using crop simulation and statistical downscaling models: a review. *Sci. Res. Essays*. **12**(18), 167–187 (2017). <https://doi.org/10.5897/SRE2017.6521>
- Chen, H., Guo, J., Zhang, Z., Xu, C.Y.: Prediction of temperature and precipitation in Sudan and South Sudan by using LARS-WG in future. *Theor. Appl. Climatol.* **113**(3–4), 363–375 (2013). <https://doi.org/10.1007/s00704-012-0793-9>
- Chu, J.T., Xia, J., Xu, C.Y., Singh, V.P.: Statistical downscaling of daily mean temperature, pan evaporation and precipitation for climate change scenarios in Haihe River, China. *Theor. Appl. Climatol.* **99**(1–2), 149–161 (2010). <https://doi.org/10.1007/s00704-009-0129-6>
- Conway, D., Wilby, R.L., Jones, P.D.: Precipitation and air flow indices over the British Isles. *Clim. Res.* **7**, 169–183 (1996). <https://doi.org/10.3354/cr007169>
- Dibike, Y.B., Coulibaly, P.: Hydrologic impact of climate change in the Saguenay watershed: comparison of downscaling methods and hydrologic models. *J. Hydrol.* **307**, 145–163 (2005). <https://doi.org/10.1016/j.jhydrol.2004.10.012>
- Dubrovský, M., Buchtele, J., Žalud, Z.: High-frequency and low-frequency variability in stochastic daily weather generator and its effect on agricultural and hydrologic modelling. *Clim. Chang.* **63**(1–2), 145–179 (2004). <https://doi.org/10.1023/B:CLIM.0000018504.99914.60>
- Gulacha, M.M., Mulungu, D.M.M.: Generation of climate change scenarios for precipitation and temperature at local scales using SDSM in Wami-Ruvu River basin Tanzania. *Phys. Chem. Earth.* **100**, 62–72 (2017). <https://doi.org/10.1016/j.pce.2016.10.003>
- Hashmi, M.Z., Shamseldin, A.Y., Melville, B.W.: Comparison of SDSM and LARS-WG for simulation and downscaling of extreme precipitation events in a watershed. *Stoch. Env. Res. Risk A.* **25**(4), 475–484 (2011). <https://doi.org/10.1007/s00477-010-0416-x>
- Hassan, Z., Shamsudin, S., Harun, S.: Application of SDSM and LARS-WG for simulating and downscaling of rainfall and temperature. *Theor. Appl. Climatol.* **116**(1–2), 243–257 (2014). <https://doi.org/10.1007/s00704-013-0951-8>
- Huang, J., Zhang, J., Zhang, Z., Xu, C., Wang, B., Yao, J.: Estimation of future precipitation change in the Yangtze River basin by using statistical downscaling method. *Stoch. Env. Res. Risk A.* **25**(6), 781–792 (2011). <https://doi.org/10.1007/s00477-010-0441-9>
- Huth, R.: Statistical downscaling of daily temperature in central Europe. *J. Clim.* **15**(13), 1731–1742 (2002). [https://doi.org/10.1175/1520-0442\(2002\)015<1731:SDODTI>2.0.CO;2](https://doi.org/10.1175/1520-0442(2002)015<1731:SDODTI>2.0.CO;2)
- Immerzeel, W.W., Van Beek, L.P.H., Bierkens, M.F.P.: Climate change will affect the Asian water towers. *Science*. **328**, 1382–1385 (2010)
- Ipcc. Climate Change 2013: The physical science basis. Contribution of working group I to the fifth assessment report of the intergovernmental panel on climate Change. Intergovernmental panel on climate Change, working group I contribution to the IPCC fifth assessment report (AR5) (Cambridge Univ press, New York), 1535 (2013). <https://doi.org/10.1029/2000JD000115>
- Khan, M.S., Coulibaly, P., Dibike, Y.: Uncertainty analysis of statistical downscaling methods. *J. Hydrol.* **319**(1–4), 357–382 (2006). <https://doi.org/10.1016/j.jhydrol.2005.06.035>
- Li, C., von Storch, J.S., Marotzke, J.: Deep-ocean heat uptake and equilibrium climate response. *Clim. Dyn.* **40**(5–6), 1071–1086 (2013). <https://doi.org/10.1007/s00382-012-1350-z>
- Mahmood, R., Babel, M.S.: Evaluation of SDSM developed by annual and monthly sub-models for downscaling temperature and precipitation in the Jhelum basin, Pakistan and India. *Theor. Appl. Climatol.* **113**(1–2), 27–44 (2013). <https://doi.org/10.1007/s00704-012-0765-0>
- Mahmood, R., Jia, S.: An extended linear scaling method for downscaling temperature and its implication in the Jhelum River basin, Pakistan, and India, using CMIP5 GCMs. *Theor. Appl. Climatol.* **130**(3–4), 725–734 (2017). <https://doi.org/10.1007/s00704-016-1918-3>
- Mahmood, R., Jia, S., Tripathi, N.K., Shrestha, S.: Precipitation extended linear scaling method for correcting GCM precipitation and its evaluation and implication in the transboundary Jhelum River basin. *Atmosphere*. **9**(5), (2018). <https://doi.org/10.3390/atmos9050160>
- Maraun, D., Wetterhall, F., Chandler, R.E., Kendon, E.J., Widmann, M., Brienen, S., ... Thiele-Eich, I.: Precipitation downscaling under climate change: recent developments to bridge the gap between dynamical models and the end user. *Rev. Geophys.*, **48**(2009RG000314), 1–38 (2010). <https://doi.org/10.1029/2009RG000314.1.INTRODUCTION>
- Mason, S.J.: Simulating climate over western North America using stochastic weather generators. *Clim. Chang.* **62**(1–3), 155–187 (2004). <https://doi.org/10.1023/B:CLIM.0000013700.12591.ca>
- Meaurio, M., Zabaleta, A., Boithias, L., Epelde, A.M., Sauvage, S., Sánchez-Pérez, J.M., ... Antiguada, I.: Assessing the hydrological response from an ensemble of CMIP5 climate projections in the transition zone of the Atlantic region (Bay of Biscay). *J. Hydrol.* **548**, 46–62 (2017). <https://doi.org/10.1016/j.jhydrol.2017.02.029>
- Meehl, G.A., Stocker, T.F., Collins, W.D., Friedlingstein, P., Gaye, A.T., Gregory, J.M., ... Zhao, Z.-C.: Global Climate Projections. Climate Change 2007: Contribution of Working Group I to the Fourth Assessment Report of the Intergovernmental Panel on Climate Change, 747–846 (2007). <https://doi.org/10.1080/07341510601092191>
- Mehan, S., Guo, T., Gitau, M., Flanagan, D.C.: Comparative study of different stochastic weather generators for long-term climate data simulation. *Climate*. **5**(2), 26 (2017). <https://doi.org/10.3390/cli5020026>
- Moss, R.H., Edmonds, J.A., Hibbard, K.A., Manning, M.R., Rose, S.K., Van Vuuren, D.P., ... Wilbanks, T. J.: The next generation of scenarios for climate change research and assessment. *Nature*, **463**(7282), 747–756 (2010). <https://doi.org/10.1038/nature08823>

- Pervez, M.S., Henebry, G.M.: Projections of the Ganges-Brahmaputra precipitation-downscaled from GCM predictors. *J. Hydrol.* **517**, 120–134 (2014). <https://doi.org/10.1016/j.jhydrol.2014.05.016>
- Peterson, T.C.: Climate Change indices. *World Meteorol. Organ. Bull.* **54**, 83–86 (2005)
- Prasanna, V.: Regional climate change scenarios over South Asia in the CMIP5 coupled climate model simulations. *Meteorol. Atmos. Phys.* **127**, 561–578 (2015)
- Sachindra, D.A., Perera, B.J.C.: Statistical downscaling of general circulation model outputs to precipitation accounting for non-stationarities in predictor-predictand relationships. *PLoS One.* **11**(12), 1–21 (2016). <https://doi.org/10.1371/journal.pone.0168701>
- Semenov, M.A., & Barrow, E.M.: A Stochastic Weather Generator for Use in Climate Impact Studies. User Manual, Hertfordshire, UK, (August), 0–27 (2002)
- Semenov, M.A., Stratonovitch, P.: Use of multi-model ensembles from global climate models for assessment of climate change impacts. *Clim. Res.* **41**(1), 1–14 (2010). <https://doi.org/10.3354/cr00836>
- Semenov, M.A., Brooks, R.J., Barrow, E.M., Richardson, C.W.: Comparison of the WGEN and LARS-WG stochastic weather generators for diverse climates. *Clim. Res.* **10**(2), 95–107 (1998). <https://doi.org/10.3354/cr010095>
- Sharma, A., Sharma, D., Panda, S.K., Dubey, S.K., Pradhan, R.K.: Investigation of temperature and its indices under climate change scenarios over different regions of Rajasthan state in India. *Glob. Planet. Chang.* **161**(December 2017), 82–96 (2018). <https://doi.org/10.1016/j.gloplacha.2017.12.008>
- Taylor, K.E.: Summarizing multiple aspects of model performance in a single diagram. *J. Geophys. Res.* **106**(D7), 7183–7192 (2001). <https://doi.org/10.1029/2000JD900719>
- Taylor, K.E., Stouffer, R.J., Meehl, G.A.: An overview of CMIP5 and the experiment design. *Bull. Am. Meteorol. Soc.* **93**(4), 485–498 (2012). <https://doi.org/10.1175/BAMS-D-11-00094.1>
- Turco, M., Quintana-Seguí, P., Llasat, M.C., Herrera, S., Gutiérrez, J.M.: Testing MOS precipitation downscaling for ENSEMBLES regional climate models over Spain. *J. Geophys. Res. Atmos.* **116**(18), 1–14 (2011). <https://doi.org/10.1029/2011JD016166>
- Wigley, T.M.L., Jones, P.D., Briffa, K.R., Smith, G.: Obtaining subgrid scale information from coarse-resolution general circulation model output. *J. Geophys. Res.* **95**, 1943–1953 (1990)
- Wilby, R., & Dawson, C.: Using SDSM version 3.1- A decision support tool for the assessment of regional climate change impacts, 17, 147–159 (2004)
- Wilby, R.L., Dawson, C.W., Barrow, E.: SDSM: a decision support tool for the assessment of regional climate change impacts. *Environ. Model. Softw.* **17**(2), 145–157 (2002)
- Wilby, R.L., Whitehead, P.G., Wade, A.J., Butterfield, D., Davis, R.J., Watts, G.: Integrated modelling of climate change impacts on water resources and quality in a lowland catchment: river Kennet, UK. *J. Hydrol.* **330**(1–2), 204–220 (2006). <https://doi.org/10.1016/j.jhydrol.2006.04.033>
- Wilks, D.S.: Multisite downscaling of daily precipitation with a stochastic weather generator. *Clim. Res.* **11**(2), 125–136 (1999). <https://doi.org/10.3354/cr011125>
- Wilks, D.S., Wilby, R.L.: The weather generation game: a review of stochastic weather models. *Prog. Phys. Geogr.* **23**(3), 329–357 (1999). <https://doi.org/10.1191/030913399666525256>
- Zhang, Y., You, Q., Chen, C., Ge, J.: Impacts of climate change on streamflows under RCP scenarios: a case study in Xin River basin, China. *Atmos. Res.* **178–179**, 521–534 (2016). <https://doi.org/10.1016/j.atmosres.2016.04.018>
- Zhou, T., Yu, R.: Twentieth-century surface air temperature over China and the globe simulated by coupled climate models. *J. Clim.* **19**(22), 5843–5858 (2006). <https://doi.org/10.1175/JCLI3952.1>

